







Article

Influence of an Antioxidant Nanomaterial on Oral Tablet Formulation: Flow Properties and Critical Quality Attributes

Andrea C. Ortiz ¹, Javiera Carrasco-Rojas ², Sofía Peñaloza ², Mario J. Simirgiotis ³, Lorena Rubio-Quiroz ⁴, Diego Ruiz ³, Carlos F. Lagos ^{4,5}, Javier Morales ^{2,*} and Francisco Arriagada ^{2,*}

¹ Escuela de Química y Farmacia, Facultad de Ciencias, Universidad San Sebastián, Santiago 7510157, Chile; andrea.ortizo@uss.cl

² Departamento de Ciencias y Tecnología Farmacéutica, Facultad de Ciencias Químicas y Farmacéuticas, Universidad de Chile, Santiago 8380494, Chile

³ Instituto de Farmacia, Facultad de Ciencias, Universidad Austral de Chile, Campus Isla Teja, Valdivia 5090000, Chile

⁴ Chemical Biology & Drug Discovery Lab, Escuela de Química y Farmacia, Facultad de Ciencias, Universidad San Sebastián, Campus Los Leones, Lota 2465 Providencia, Santiago 7510157, Chile

⁵ Centro Basal Ciencia & Vida, Fundación Ciencia & Vida, Av. del Valle Norte 725, Huechuraba 8580702, Chile

* Correspondence: javiermv@ciq.uchile.cl (J.M.); francisco.arriagada@ciq.uchile.cl (F.A.)

Abstract

Antioxidant nanomaterials, particularly mesoporous silica nanoparticles (MSNs) functionalized with polyphenols, offer innovative solutions for protecting oxidation-sensitive components and enhancing bioavailability in pharmaceuticals or extending the shelf life of nutraceutical and food products. This study investigates the influence of MSNs functionalized with caffeic acid (MSN-CAF) on powder flow properties and their tableting performance. Aminated MSNs were synthesized via co-condensation and conjugated with caffeic acid using EDC/NHS chemistry. Antioxidant capacity was evaluated using DPPH[•], ABTS^{•+}, ORAC, and FRAP assays. Powder blends with varying MSN-CAF concentrations (10–70%) were characterized for flow properties (angle of repose, Hausner ratio, Carr's index), tablets were produced via direct compression, and critical quality attributes (weight uniformity, hardness, friability, disintegration, nanoparticle release) were assessed. MSN-CAF exhibited reduced antioxidant capacity compared with free caffeic acid due to pore entrapment but retained significant activity. Formulation F1 (10% MSN-CAF) showed excellent flowability (angle of repose: 12°, Hausner ratio: 1.16, Carr's index: 14%), enabling robust tablet production with rapid disintegration, low friability, and complete nanoparticle release in 10 min. Additionally, the antioxidant nanomaterial demonstrated biocompatibility with the HepG2 cell line. MSN-CAF is a versatile nanoexcipient for direct compression tablets, offering potential as an active packaging agent and delivery system in the nutraceutical and food industries.

Keywords: antioxidant nanomaterial; nanoantioxidant; mesoporous silica nanoparticles; caffeic acid; powder flow properties; antioxidant tablets



Academic Editor: María Jesús Petrón Testón

Received: 31 May 2025

Revised: 29 June 2025

Accepted: 3 July 2025

Published: 5 July 2025

Citation: Ortiz, A.C.; Carrasco-Rojas, J.; Peñaloza, S.; Simirgiotis, M.J.; Rubio-Quiroz, L.; Ruiz, D.; Lagos, C.F.; Morales, J.; Arriagada, F. Influence of an Antioxidant Nanomaterial on Oral Tablet Formulation: Flow Properties and Critical Quality Attributes. *Antioxidants* **2025**, *14*, 829. <https://doi.org/10.3390/antiox14070829>

Copyright: © 2025 by the authors. Licensee MDPI, Basel, Switzerland. This article is an open access article distributed under the terms and conditions of the Creative Commons Attribution (CC BY) license (<https://creativecommons.org/licenses/by/4.0/>).

1. Introduction

Surface-functionalized nanoparticles with antioxidants, also known as nanoantioxidants, have emerged as a new generation of antioxidant agents [1,2]. These systems overcome significant limitations of natural antioxidants, which are prone to activity loss during processing or storage because of their sensitivity to pH, light, oxygen, and heat [3].

Additionally, they can enhance the transport and dissolution rate of poorly water-soluble polyphenols, thereby improving bioavailability [4,5]. Consequently, antioxidant nanomaterials have been investigated for applications in biomedicine, the pharmaceutical industry, cosmetics, the food industry, and nutraceuticals [6–10]. In particular, silica-based antioxidant nanomaterials have garnered significant interest due to the unique properties of the silica matrix. Silicon dioxide nanoparticles possess a highly versatile surface that enables the incorporation of functional groups, facilitating covalent bonding or physical adsorption of various polyphenols. These surface advantages, combined with the versatility of the silica matrix, allow for the modification of particles to achieve porosity, a hollow cavity to encapsulate bioactive molecules, or degradability in response to specific stimuli. Furthermore, colloidal silicon dioxide is classified as a Generally Recognized as Safe (GRAS) material and is used as a food additive (E-551). However, mesoporous silica nanoparticles (MSNs) as drug delivery carriers have not been commercialized in the pharmaceutical industry, though they have been extensively studied [11,12]. Notably, their incorporation into oral tablets has been reported. Ibrahim A. H. and colleagues utilized a 3^2 full factorial design to optimize a formulation containing silymarin-loaded MSNs for the production of lyophilized tablets [13]. Similarly, Kim D. et al. reported tablets containing celecoxib-loaded MSNs to enhance drug loading and subsequent dissolution [14]. Additionally, Abbaraju P. et al. used MCM-41 particles to fabricate floating tablets [15]. However, despite reports of MSN incorporation into tablets, critical technological parameters for their formulation remain underexplored. Powder flow properties are influenced by (i) steric repulsions, (ii) friction forces, and (iii) cohesive forces [16]. On one hand, steric repulsion and cohesive forces are associated with grain geometry and interactions such as liquid bridges, electrostatic charges, magnetic dipole–dipole interactions, or van der Waals forces, respectively. On the other hand, friction forces depend on both the surface state (rough or smooth) and the chemical nature of the powders [17]. The predominance of one of these forces over the others results from the microenvironmental conditions and the physicochemical properties of the grains. When nanoparticles are blended with different excipient powders, the nanoparticles are expected to adsorb onto the surface of the powder particles, with either homogeneous or heterogeneous dispersion. In this context, the distribution is primarily influenced by the surface properties of the nanoparticles. The hydrophobic or hydrophilic nature of antioxidants in nanomaterials can influence their interparticle interactions, which in turn affect the final rheological properties of the powder. However, limited studies are available on the influence of mesoporous silica nanoparticles on powder flow properties, and even fewer address antioxidant nanomaterials. To the best of our knowledge, there are no reports on the incorporation of silica-based nanoantioxidants into oral tablets. Because of their properties, MSN-based antioxidant nanomaterials can serve as nanoexcipients to protect oxidation-sensitive components in formulations, nanocarriers to enhance the apparent solubility and transport of bioactive molecules across membranes, and agents with inherent antioxidant activity. This is of significant importance in the pharmaceutical, cosmetic, and nutraceutical industries, adding value to formulations and extending product shelf life by acting as an active packaging agent.

Here, we investigated the influence of a silica-based antioxidant nanomaterial on the rheological properties of powders blends used to produce oral tablets by direct compression. To this end, we synthesized, using a cocondensation method, aminated porous silica nanoparticles onto which caffeic acid was immobilized. Caffeic acid is a naturally occurring polyphenol found in a wide variety of plants, including coffee, fruits, and vegetables [18]. It is one of the most potent antioxidants within the hydroxycinnamic acid family [19] and the predominant member of that family in the human diet [20], being linked to various pharmacological benefits [21–23]. In addition to the above, which highlights its importance and

interest for conjugation as an antioxidant molecule, it offers several operational advantages. Among these, its relatively hydrophilic nature stands out, facilitating its incorporation into aqueous solutions; it possesses structural simplicity compared with other antioxidant molecules, such as flavonoids; and it features a carboxylic group, which enables its direct conjugation to various surfaces [24–27]. Although the antioxidant activity of caffeic acid is known to rely on both its catechol group and acrylic acid moiety [28], the literature suggests that the contribution of the carboxylic acid is moderate compared with that of the catechol [29,30]. Therefore, conjugation via this functional group may ensure that its activity is not drastically reduced. These characteristics make caffeic acid an attractive molecule for easy incorporation onto the surface of nanomaterials, which is why it was selected. This antioxidant nanomaterial was thoroughly characterized, and its antioxidant capacity was evaluated using DPPH•, ABTS•+, ORAC, and FRAP assays. The influence of this nanomaterial on the flow properties of a powder for direct compression was assessed by varying the proportion of the antioxidant nanomaterial and other excipients. From a formulation with optimal properties, oral tablets containing the antioxidant nanomaterial were manufactured, and their critical quality attributes were evaluated.

2. Materials and Methods

Tetraethyl orthosilicate (TEOS, 98%), and (3-aminopropyl)triethoxysilane (APTES, ≥98%), caffeic acid (CAF, ≥98%), ethyl-3-(3-dimethylaminopropyl)carbodiimide (EDC, ≥98%), *n*-hydroxysuccinimide (NHS, 98%), ammonium hydroxide solution (NH₄OH, 28–30%, ACS reagent), Folin–Ciocâlțeu reagent, 2,2-diphenyl-1-picrylhydrazyl (DPPH•), 2,2'-azino-bis-(3-ethylbenzothiazoline-6-sulfonic acid (ABTS), fluorescein, 2,2'-Azobis(2-methylpropionamide) dihydrochloride (AAPH, 97%), and 2,4,6-tripyridyl-*s*-triazine (TPTZ, ≥98%) were purchased from Merck (Merck KGaA, Darmstadt, Germany). Cetyltrimethylammonium bromide (CTAB, 99%), hydrochloric acid fuming (HCl, 37%, ACS grade), and absolute ethanol (EtOH, ACS grade) were obtained from PanReac AppliChem ITW Reagents (Darmstadt, Germany). All reagents were used without prior purification. All experiments were carried out using deionized water (Milli-Q, 18.2 MΩ·cm).

2.1. Antioxidant Nanomaterial Synthesis

2.1.1. Synthesis of Aminofunctionalized Mesoporous Silica Nanoparticles (MSN-NH₂)

For the synthesis of MSN-NH₂, a previously reported co-condensation method was modified [31]. In a round-bottom flask, 0.82 g of CTAB was dissolved in 560 mL of water at 40 °C. After the temperature reached 25 °C, the mixture was stirred for 45 min. Then, a mixture of APTES (1.8 mL) and TEOS (6.9 mL) was added dropwise to the aqueous solution of CTAB. Subsequently, 4.5 mL of NH₄OH (25%) was added and allowed to react for 4 h at room temperature with constant stirring. The MSN-NH₂ was collected by centrifugation and washed thoroughly. The surfactant was removed by solvent extraction, leaving the nanoparticles suspended in an acidic ethanol solution (0.6 M HCl) under constant stirring and reflux for 6 h. Finally, three washes with water and one with ethanol were performed. This process was performed twice.

2.1.2. Functionalization of MSN-NH₂ with Caffeic Acid (MSN-CAF)

The MSN-NH₂ was surface functionalized with caffeic acid following a previously reported method [32]. Briefly, in a round-bottom flask CAF (11.1 mM), EDC (22.2 mM), and NHS (44.4 mM) were dissolved in water, using ethanol as cosolvent. The mixture was stirred for 10 min, after which an aqueous nanoparticle suspension (10 mg/mL) was added. The reaction mixture was then allowed to proceed for 6 h at room temperature. The nanoparticles conjugated with CAF (MSN-CAF), i.e., antioxidant nanomaterials, were

collected by centrifugation and washed. They were then dried at 60 °C under vacuum for 12 h and collected as powder.

2.2. Preparation of Tablet Formulation

The tablet formulation (125 mg) consisted of MicroceLac[®] 100 (75% alpha-lactose monohydrate and 25% microcrystalline cellulose), crospovidone, magnesium stearate, and the antioxidant nanomaterial (or MSN-NH₂ as control). These materials were selected because they are among the most commonly used excipients in tablet compression processes, ensuring robustness and reproducibility in formulation development [33]. Briefly, MicroceLac[®] 100 was selected as a coprocessed excipient that combines lactose and microcrystalline cellulose, offering both good compressibility and improved flow properties, which are essential for direct compression [34]. Crospovidone was included as a superdisintegrant to promote rapid tablet disintegration [35], and magnesium stearate was selected as a lubricant to prevent sticking and ensure good flow during tableting [36,37]. Given that crospovidone is typically used at 2–5% in tablet formulations, with changes in its proportion causing significant variations in disintegration time [38,39], we maintained its concentration as constant to isolate and evaluate the effects specifically associated with varying nanoparticle proportions. Additionally, to maintain appropriate tablet weight and ensure adequate lubrication for proper compression, the proportions of MicroceLac[®] 100 and magnesium stearate were adjusted accordingly.

The impact of the antioxidant nanomaterial on the angle of repose, flowability, and compressibility properties was assessed by varying the ratio of MSN-CAF (or MSN-NH₂) to MicroceLac in four different formulations (Table 1). All powders in the formulation were mixed manually [40].

Table 1. Compositions of the tablet formulations containing antioxidant nanomaterial and MSN-NH₂.

Excipients	F1 (%)	F2 (%)	F3 (%)	F4 (%)	N1 (%)	N2 (%)	N3 (%)	N4 (%)
MSN-NH ₂	-	-	-	-	10.0	27.5	50.0	70.0
MSN-CAF	10.0	27.5	50.0	70.0	-	-	-	-
MicroceLac [®] 100	87.5	70	47.5	27.5	87.5	70	47.5	27.5
Crospovidone	2.0	2.0	2.0	2.0	2.0	2.0	2.0	2.0
Magnesium stearate	0.5	0.5	0.5	0.5	0.5	0.5	0.5	0.5
Total	100	100	100	100	100	100	100	100

2.3. Materials Characterization

The hydrodynamic diameter and zeta potential of the nanoantioxidant were measured in triplicate using a Zetasizer Nano ZS90 (Malvern, London, UK), with a detection angle of 173° and an equilibration time of 120 s. Textural properties such as specific surface and pore volume of the nanomaterials were calculated by the Brunauer–Emmett–Teller (BET) and Barrett–Joyner–Halenda (BJH) methods, using a N₂ adsorption/desorption isotherm measured at −196 °C on a Micromeritics 3-Flex instrument (Micromeritics Instruments, Norcross, GA, USA). FT-IR was used to analyze the vibrational modes of the characteristic functional groups of MSN-NH₂ and MSN-CAF. Infrared spectra were obtained using a Nicolet iS5 FT-IR spectrometer (Nicolet Instrument, Thermo Fisher Scientific, Waltham, MA, USA) in the range 650 to 4000 cm^{−1}, with a resolution of 4 cm^{−1} and 16 scans per spectrum to generate an average. To analyze the shape and surface of samples (nanoantioxidant, powder, and tablet), scanning electron microscopy (SEM) images were taken on an FEI inspect F50 model microscope (FEI, Hillsboro, OR, USA) with an accelerating voltage of 10.00 kV. Thermogravimetric analysis (TGA) was conducted using a Netzsch TG

209 F1 (Netzsch-Gerätebau GmbH, Selb, Germany) with an airflow of 20 mL/min and a heating rate of 10 °C/min, over a temperature range of 30–800 °C.

Nanoantioxidant samples were suspended in ethanol. An aliquot was taken and deposited onto a silicon grid, dried, and then coated with gold. The powder blend or tablet samples were deposited directly on the grid and then coated with gold.

2.4. Characterization of Antioxidant Activity and Total Phenolic Content

2.4.1. Determination of Total Phenolic Content

The total phenolic content (TPC) was determined using the Folin–Ciocâlțeu method [41]. Each sample was dissolved (or suspended in the case of nanoparticle samples) in distilled water and mixed with 10% Folin–Ciocâlțeu reagent, followed by incubation for 2 min at 40 °C. Subsequently, 5% Na₂CO₃ was added, and the mixture was incubated for an additional 20 min at 40 °C. The absorbance of the samples was measured at 765 nm using a microplate reader (BioTek Instruments, Inc., Winooski, VT, USA). The results are expressed as milligrams of gallic acid equivalents per gram of powder (mg GAE/g powder).

2.4.2. DPPH Radical Scavenging Assay

The concentration required to scavenge 50% of the DPPH radical (SC₅₀) was determined. Briefly, 50 μL of the sample (free CAF or antioxidant nanomaterial) was mixed with 150 μL of a DPPH• solution in ethanol (156 μM) and incubated for 30 min in the dark. The absorbance was then measured at 517 nm using a microplate reader. The results were expressed as μg/mL [42].

2.4.3. ABTS•+ Scavenging Assay

The concentration required to scavenge 50% of the ABTS radical (SC₅₀) was determined. Briefly, 50 μL of each sample was mixed with 150 μL of a 169 μM ABTS radical solution and incubated for 30 min in the dark. The absorbance was measured at 732 nm using a microplate reader. Similarly as for the DPPH• assay, the results were expressed as μg/mL [43].

2.4.4. Oxygen Radical Absorbance Capacity (ORAC) Assay

The ORAC assay was performed using a microplate reader as previously described [42]. Briefly, 45 μL of the sample and 175 μL of a fluorescein solution (108 nM) were pre-incubated for 30 min at 37 °C. Then, 50 μL of AAPH (18 mM) was added to the mixture, and the fluorescence was measured every 2 min for 2 h at excitation and emission wavelengths of 480 nm and 520 nm, respectively. The results are expressed as micromoles of Trolox per gram of powder (μmol Trolox/g powder).

2.4.5. Ferric-Reducing Antioxidant Power (FRAP) Assay

The FRAP assay, based on the reduction of Fe³⁺-TPTZ to Fe²⁺-TPTZ, was performed using a microplate reader following established procedures [43]. Briefly, 10 μL of the sample was mixed with 290 μL of FRAP reagent, and the mixture was incubated for 60 min in the dark. The absorbance was then measured at 593 nm. The results were expressed as micromoles of Trolox per gram of powder (μmol Trolox/g powder).

2.5. Rheological Properties

2.5.1. Angle of Repose

The static angle of repose (θ) was determined according to USP specifications using a funnel positioned 4 cm from the top of the cone-like pile of powder sample. After the

powder flowed through the funnel, the angle of repose for each sample was calculated using Equation (1). The test was conducted in triplicate ($n = 3$).

$$\tan \theta = \frac{\text{Height (cm)}}{\text{Radius (cm)}} \quad (1)$$

2.5.2. Powder Flowability

The flowability of powder mixtures was evaluated using the Hausner ratio (Equation (2)) and the compressibility index (Carr's index, Equation (3)). Measurements of bulk and tapped volumes were performed with an ETD-1020 tap density tester (Electrolab, Mumbai, India). Powder mixtures were placed in a graduated cylinder, and the untapped bulk volume (V_0 , mL) was recorded. After 500 taps, the final tapped volume (V_f , mL) was measured. The test was conducted in triplicate ($n = 3$).

$$\text{Hausner ratio} = \frac{V_0}{V_f} \quad (2)$$

$$\text{Compressibility Index} = \frac{V_0 - V_f}{V_0} \times 100 \quad (3)$$

The flow properties were classified according to the criteria outlined in USP <1174> (2024) [44], based on the angle of repose, Hausner ratio, and Carr's index values, as presented in Table 2.

Table 2. Flow properties corresponding to the angle of repose, Hausner ratio, and compressibility index.

Angle of Repose	Hausner Ratio	Compressibility Index	Flow Characteristic
25–30	1.00–1.11	1–10	Excellent
31–35	1.12–1.18	11–15	Good
36–40	1.19–1.25	16–20	Fair
41–45	1.26–1.34	21–25	Passable
46–55	1.35–1.45	26–31	Poor
56–65	1.46–1.59	32–37	Very poor
>66	>1.60	>38	Very, very poor

2.6. Tablets Manufacturing

The tablets were manufactured by direct compression of the previously described powder blend. The process was carried out using D-type punches with a diameter of 5 mm. The compression speed was set to level 3, and the compression hardness to level 5, using a D-8 Piccola Classica rotary tablet press (Riva, Buenos Aires, Argentina). In each compression batch, the first 10 tablets were discarded.

2.7. Characterization of the Critical Quality Attributes of the Final Product

2.7.1. Weight Uniformity and Tablet Dimensions

Weight uniformity was assessed in accordance with the specifications outlined in the monograph for each finished product. As no active pharmaceutical ingredient was used in this study, no specific weight uniformity requirements were stipulated. However, based on the punch type used during manufacturing, a target tablet weight of 120 mg (with an acceptable range of 90–110%) was optimized. After tablet production, 10 tablets were randomly selected and individually weighed using an analytical balance. Tablet dimensions were measured using a vernier caliper. The diameter was determined by positioning the caliper jaws around the tablet's circumference, while the thickness was measured between the flat surfaces.

2.7.2. Tablet Hardness

Tablet hardness was evaluated using a durometer (Erweka, Langen, Germany). The assessment was conducted on each production batch, with 10 tablets randomly selected for testing.

2.7.3. Friability Test

Friability was evaluated according to USP (2024). For tablets with a unit mass of 650 mg or less, a sample of whole tablets equivalent to approximately 6.5 g was used. For tablets with a unit mass greater than 650 mg, 10 whole tablets were selected. Before testing, the tablets were carefully dedusted, weighed, and placed in the drum of a friability tester. The test was conducted by rotating the drum 100 times. After testing, the tablets were removed, dedusted, and accurately weighed. Friability was calculated using Equation (4), with an acceptance criterion of weight loss of less than 1%.

$$\text{Friability (\%)} = \frac{\text{Initial weight} - \text{final weight}}{\text{Initial weight}} \times 100 \quad (4)$$

2.7.4. Disintegration Time

Disintegration was assessed in 900 mL of phosphate buffer (pH 6.8) at 37.0 ± 0.5 °C using six tablets. The disintegration time was recorded for each tablet. The test was performed using a two-bowl disintegrator with six tablet compartments (Erweka, Germany).

2.7.5. Nanoparticle Release Test

An in vitro release study was adapted to investigate the release behavior of nanoparticles from an oral tablet using a stirring technique. The release medium consisted of 10 mL of buffer solutions at pH 1.2, 4.5, and 6.8, maintained at 37 °C, based on reported procedures [45–47]. The buffer compositions are shown in Table 3.

Table 3. Buffer compositions (1 L) for release tests at pH 1.2, 4.5, and 6.8.

Component	pH 1.2	pH 4.5	pH 6.8
Sodium chloride	2.0 g	-	-
Hydrochloric acid	7.0 mL	-	-
Sodium acetate	-	2.99 g	-
Glacial acetic acid	-	1.66 mL	-
Anhydrous dibasic sodium phosphate	-	-	21.72 g
Citric acid monohydrate	-	-	4.94 g
Water	q.s. 1000 mL	q.s. 1000 mL	q.s. 1000 mL

At specific time points (2, 5, 10, 15, 20, 30, 45, and 60 min), 1 mL aliquots of the release medium were withdrawn and replaced with an equal volume of fresh medium. The collected samples were sonicated, filtered, and then centrifuged at 13,000 rpm for 20 min. The resulting nanoparticle pellet was dried and weighed to determine the cumulative release of nanoparticles at each time point.

2.8. Assessment of Cellular Metabolic Activity

The human hepatocellular carcinoma line HepG2 (ATCC HB-806) was expanded in high-glucose DMEM (Cytiva, Marlborough, MA, USA, cat. SH30243.02) containing 10% fetal bovine serum (Cytiva, cat. SV30160.03) and 1% penicillin/streptomycin (Cytiva, cat. SH40003.01). Cultures were maintained at 37 °C in a humidified 5% CO₂ incubator. Once cells reached ~90% confluence, they were washed twice with PBS (0.0067 M phosphate, Cytiva, cat. SH302560.1) and detached with 0.25% trypsin-EDTA (Corning, New York, NY,

USA, cat. 25-053-CI). A total of 1×10^4 cells were dispensed into each well of 96-well microplates (NEST Biotechnology, Wuxi, China, cat. 701001) and allowed to attach overnight. The following day, cells were treated with MSN-NH₂ or MSN-CAF at concentrations of 5, 10, 25, 50, 75, and 100 µg/mL (three independent experiments, each performed in triplicate). After 24 h or 48 h of exposure, metabolic activity was quantified with the MTT reduction assay (Sigma-Aldrich, cat. M5655, St. Louis, MO, USA). MTT was added to a final concentration of 0.5 mg/mL, and plates were incubated for 90 min at 37 °C. Formazan crystals were dissolved in dimethyl sulfoxide (DMSO) (Sigma-Aldrich, cat. D8418, St. Louis, MO, USA), and absorbance was recorded at 570 nm on a Synergy H1 reader (BioTek, Winooski, VT, USA) after 2 min of orbital shaking.

2.9. Statistical Analysis

Results are expressed as the mean \pm SD of three independent experiments, unless otherwise specified by USP guidelines. Statistical significance was determined at $p < 0.05$ using one-way or two-way ANOVA, as appropriate, followed by Tukey's post hoc test, performed with GraphPad Prism version 8.0.1 (San Diego, CA, USA).

3. Results and Discussion

3.1. Characterization of Antioxidant Nanomaterial

Antioxidant nanomaterials were synthesized via a co-condensation method using TEOS and APTES in a 4:1 ratio, followed by conjugation of caffeic acid to the surface using EDC/NHS chemistry. Physicochemical and textural properties are summarized in Table 4. Monodisperse MSN-NH₂ samples were obtained with a hydrodynamic diameter of 260 nm and a PDI of 0.15. This was corroborated by SEM images, which revealed spherical particles with an average size of 128 nm (Figure 1a). The zeta potential was +32.5 mV, indicating good colloidal stability attributed to the ionization of amino groups. The N₂ adsorption-desorption isotherm exhibited a characteristic type IV isotherm indicative of mesoporous materials (Figure 1c). The textural properties of these starting materials included a specific surface area of 542 m²/g, a pore diameter of 2.5 nm, and a pore volume of 0.41 cm³/g.

Table 4. Physicochemical and textural properties of the synthesized nanomaterials.

Sample	Hydrodynamic Diameter (nm)	Zeta Potential (mV)	Specific Surface Area (m ² /g)	Pore Diameter (nm)	Pore Volume (cm ³ /g)
MSN-NH ₂	260	+32.5	542	2.5	0.41
MSN-CAF	207	+11.8	301	2.6	0.32

Conjugation of caffeic acid, achieved through amide bond formation between the carboxylic acid group of caffeic acid and the amine groups on the silica nanoparticles, yielded ca. 12.1 mg of caffeic acid per 100 mg of nanoparticles (Figure 1d). This value was consistent with previous reports [32]. The resulting nanoantioxidant exhibited a hydrodynamic diameter of 207 nm and a zeta potential of +11.8 mV, indicating partial neutralization of the amino groups and successful conjugation. SEM images revealed no significant changes in nanoparticle morphology and size (Figure 1b). However, the specific surface area and pore volume decreased to 301 m²/g and 0.32 cm³/g, respectively. On the other hand, FTIR analysis revealed characteristic peaks that confirmed caffeic acid conjugation (Figure 1e). The spectrum of MSN-NH₂ showed a peak at 1052 cm⁻¹, corresponding to siloxane groups, and two weak peaks at 3370 cm⁻¹ and 3308 cm⁻¹, attributed to primary amine stretching vibrations. Additionally, the spectrum showed peaks at 2936 cm⁻¹ and 2868 cm⁻¹, attributed to the propyl chain, and a peak at 1595 cm⁻¹, characteristic of N-H bending [48]. The intensity of this amine group peak was notably

reduced in the nanoantioxidant spectrum, accompanied by the appearance of characteristic bands indicative of amide bond formation at 1653 cm^{-1} and 1560 cm^{-1} . In addition, a band centered at 3290 cm^{-1} suggested the presence of aromatic $-\text{OH}$ vibrations due to the catechol moiety in caffeic acid. Furthermore, bands attributable to aromatic stretching ($\text{C}=\text{C}$) in the range of $1460\text{--}1320\text{ cm}^{-1}$ confirmed the presence of caffeic acid.

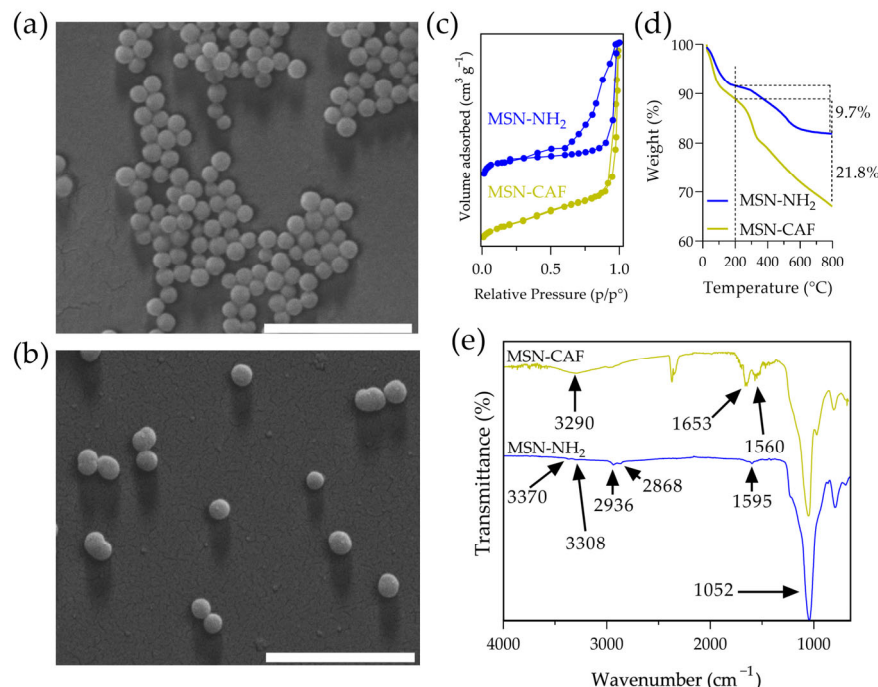


Figure 1. Characterization of nanomaterials. SEM images of (a) MSN-NH₂ and (b) MSN-CAF, (c) N₂ adsorption–desorption isotherm of nanomaterials, (d) TGA of nanomaterials, and (e) FTIR of nanomaterials. Scale bar: 1 μm .

The antioxidant properties of free caffeic acid (CAF) and the antioxidant nanomaterial (MSN-CAF) were characterized using widely validated methods, including total phenolic content (TPC), DPPH \bullet , ABTS \bullet^+ , ORAC, and FRAP assays. The results are presented in Table 5.

Table 5. Antioxidant characterization of nanomaterials. All experiments were performed in triplicate ($n = 3$).

Sample	Antioxidant Characterization				
	TPC ^a	DPPH \bullet SC ₅₀ ^b	ABTS \bullet^+ SC ₅₀ ^b	ORAC ^c	FRAP ^c
CAF	47.50 \pm 0.02	6.19 \pm 0.01	6.02 \pm 0.01	2083.6 \pm 3.8	237.8 \pm 0.01
MSN-CAF	16.00 \pm 0.01	86.60 \pm 0.01	60.50 \pm 0.01	219.6 \pm 4.8	46.80 \pm 0.01

^a expressed as mg GAE/g MSN-CAF, ^b expressed as $\mu\text{g}/\text{mL}$, ^c expressed as $\mu\text{mol Trolox}/\text{g MSN-CAF}$.

The TPC was determined to be 47.5 mg GAE/g for free CAF and 16.0 mg GAE/g for MSN-CAF. In contrast, the TPC for caffeic acid immobilized on the silica surface of MSN-CAF was approximately three times lower. This reduction was expected, as the caffeic acid content was “diluted” within the total mass of the nanomaterial, unlike free CAF, which is a pure polyphenol. The lower TPC in MSN-CAF likely resulted from both the reduced proportion of CAF and its limited availability to react with the Folin-Ciocalteu reagent.

The DPPH \bullet and ABTS \bullet^+ assays were quantified using SC₅₀ values, where a lower SC₅₀ indicates greater antiradical capacity. Free CAF exhibited SC₅₀ values of 6.19 $\mu\text{g}/\text{mL}$ (DPPH \bullet) and 6.02 $\mu\text{g}/\text{mL}$ (ABTS \bullet^+), reflecting its potent antiradical activity. However,

when conjugated to nanoparticles in MSN-CAF, the SC_{50} values increased significantly to 86.6 $\mu\text{g}/\text{mL}$ (DPPH \bullet) and 60.5 $\mu\text{g}/\text{mL}$ (ABTS), representing a 10- to 14-fold reduction in antiradical efficiency. These findings suggest that the conjugated form of CAF in MSN-CAF is less effective at scavenging free radicals. Similar trends have been observed by other researchers studying CAF [32,49], gallic acid [50], epigallocatechin-3-gallate [51], and kaempferol [52] incorporated into mesoporous silica nanoparticles (MSNs).

The antiradical activity of caffeic acid is widely attributed to hydrogen atom transfer (HAT) and single electron transfer (SET) mechanisms, with HAT being predominant [19,53–55]. This scavenging effect relies on the catechol group in caffeic acid, supported by the stabilizing effects of the benzene ring, the conjugated double bond, and the carboxyl group [56]. However, steric hindrance caused by the nanoparticle limits the accessibility of DPPH \bullet and ABTS \bullet^+ molecules to CAF, reducing reaction efficiency [55,57]. This restricted diffusion of reactants (DPPH, ABTS, and caffeic acid) is the primary cause of the diminished antioxidant activity in MSN-CAF. Nevertheless, the nanomaterial retained significant radical-scavenging capacity. Conversely, some studies have reported enhanced antiradical capacity when polyphenols are incorporated into nanomaterials [58–60], though this is often due to the release of antioxidants from the matrix.

The ORAC and FRAP assays assess the ability of samples to inhibit fluorescein oxidation by reactive oxygen species (ROS) and to reduce the ferric tripyridyltriazine complex to its ferrous form, respectively. Free CAF demonstrated high antioxidant capacity with ORAC = 2083.6 $\mu\text{mol Trolox}/\text{g}$ and FRAP = 237.8 $\mu\text{mol Trolox}/\text{g}$. In contrast, MSN-CAF showed reduced values of ORAC = 219.6 $\mu\text{mol Trolox}/\text{g}$ and FRAP = 46.8 $\mu\text{mol Trolox}/\text{g}$, reflecting five- and ninefold decreases in antioxidant capacity for FRAP and ORAC, respectively. The consistent reduction in antioxidant capacity across all assays for MSN-CAF can be attributed to three main factors: (1) conjugation effects, such as amide bond formation, which eliminates the carboxyl group's contribution to antioxidant activity; (2) the proportion of caffeic acid available on the nanoparticle surface relative to that within its pores; (3) limited molecular interactions due to restricted diffusion.

Despite this attenuation, the MSN-CAF antioxidant activity suggests potential for protecting oxidation-sensitive molecules in applications such as biomedicine, pharmaceuticals, cosmetics, or food industries, enhancing product shelf life. Notably, the starting material, MSN-NH $_2$, exhibited no significant antioxidant capacity, as previously reported [51,61]. Thus, the observed antioxidant properties of MSN-CAF are directly attributable to the successful conjugation of caffeic acid.

3.2. Effect of Nanoparticles on the Rheological Properties of Blended Powders

Tablet formulation requires a minimal set of essential excipients that, together with the active pharmaceutical ingredients (APIs) or bioactive ingredients, ensure adequate powder flowability and compressibility. Generally, direct compression tablet production necessitates the inclusion of a filler, a binder, and a disintegrant; additionally, from an operational perspective, a lubricant is typically required. Based on its established use in pharmaceutical formulations and favorable properties for direct compression [62–64], MicroceLac[®] 100 (a coprocessed filler/binder composed of 75% lactose monohydrate and 25% microcrystalline cellulose), crospovidone (superdisintegrant, 2%), and magnesium stearate (lubricant/glidant, 0.5%) were selected as excipients in addition to the antioxidant nanomaterial. Furthermore, the nonionized nature of crospovidone minimizes the potential for incompatibilities with the nanoparticles.

Powder flowability is a critical factor influencing the manufacturing of tablets produced by direct compression. Accordingly, the excipients and the excipient mixtures with MSN-NH $_2$ and MSN-CAF were characterized based on their rheological parameters to

ensure adequate flowability for direct compression. Initially, the influence of the antioxidant nanomaterial on the rheological properties of the blended powders was investigated. To this end, the angle of repose, Hausner ratio, and Carr's index were evaluated for the MSN-CAF nanoparticle powder alone. The angle of repose reflects the degree of interparticle friction or resistance to powder flow. On the other hand, the Hausner ratio and Carr's index are empirically derived parameters used to evaluate powder flowability based on bulk density measurements [65]. The Hausner ratio serves as a measure of frictional forces between powder particles, while Carr's index, also known as the compressibility index, quantifies a powder's tendency to consolidate, derived from the difference between bulk and tapped densities. These parameters highlight the significance of interparticle interactions, which are typically minimal in free-flowing powders, resulting in similar bulk and tapped density values [37].

The MSN-CAF nanoparticle powder displayed an angle of repose of 62° , aligning with a Hausner ratio of 1.51 and a Carr's index of 34, indicating very poor flow properties (Table 6). A similar pattern was observed for MSN-NH₂. Bare mesoporous silica nanoparticles (MSNs) generally exhibit hydrophilic nature due to surface silanol (–OH) groups. The starting material in this work, MSN-NH₂, comprises aminated nanoparticles, which have predominantly aminopropyl moieties on their surface and within pores, alongside residual silanols from TEOS. After conjugation with caffeic acid, partial neutralization of amino groups was observed, likely resulting from amide bond formation. This suggests the coexistence of silanol (–OH), amino (–NH₂), and caffeic acid moieties on the nanoparticle surface. However, the propyl chain from APTES, the amide bonds formed during conjugation, and the benzene ring of caffeic acid confer a degree of hydrophobicity relative to bare MSNs, leading to slight particle aggregation. Furthermore, residual –NH₂ groups (due to incomplete functionalization) and catechol groups from caffeic acid may enhance interparticle interactions. These characteristics underscore the necessity of blending MSN-CAF with suitable excipients to facilitate its use in the formulation of oral tablets. Previous studies have similarly reported elevated angles of repose ($\geq 40^\circ$) for silica-based materials alone, which is consistent with our results [66–68]. In the formulated blends, magnesium stearate and croscopovidone were incorporated at a constant low concentration. The ratio of MSN-CAF (or MSN-NH₂) to MicroceLac[®] 100 was varied, as detailed in Table 1, yielding four formulations for MSN-CAF (F1–F4) and four formulations for MSN-NH₂ (N1–N4). Blending the antioxidant nanomaterial with excipients altered the flow properties, as presented in Table 6. Furthermore, a blend of excipients alone (MicroceLac[®] 100, croscopovidone, and magnesium stearate) was evaluated as a control to assess the influence of nanomaterials on flow properties and was designated as B0. This sample (B0) exhibited excellent to good flow properties.

Formulation F4, with 70% MSN-CAF, exhibited flow properties classified as poor to very, very poor. Likewise, formulation F3, containing 50% MSN-CAF, showed a fair angle of repose but very poor Hausner ratio and Carr's index values. In contrast, formulation F2, with 27.5% MSN-CAF, achieved an angle of repose of 25° , categorized as excellent, with Hausner ratio and Carr's index values rated as passable. At the lowest MSN-CAF concentration of 10% (F1), the angle of repose was 12° , with a Hausner ratio of 1.16 and a Carr's index of 14%. These values for F1 indicate excellent flowability, characterized by low cohesiveness and free-flowing behavior, suggesting a system with good consolidation and minimal interparticle friction. This facilitates handling in automated systems such as hoppers, conveyors, or tablet compression equipment. Similarly, formulations N1 to N4 exhibited results that followed the same trend. This behavior underscores that, under our experimental conditions, the antioxidant nanomaterial significantly influenced powder flow properties, with the nanoparticle itself exerting a greater impact than the antioxidant. This

can be explained by the fact that caffeic acid, in addition to being conjugated on the surface, is located within the pores, reducing its surface presence, which is in concordance with the antioxidant capacity characterization. Further experiments using a broader range of antioxidants with varying hydrophilic/hydrophobic properties and/or nonporous compact silica nanoparticles could provide deeper insights into these results. Nevertheless, the influence of the antioxidant nanomaterial on powder flow properties was evident and can be attributed to MSN-CAF enhancing interparticle attractive forces, promoting aggregation, and increasing cohesiveness and flow resistance. Formulations F3 and F4, exhibiting poor flowability, high cohesiveness, and limited compaction capacity, may present challenges in industrial-scale material handling and processing. From a technological perspective, only formulations F1 and F2 are suitable for pharmaceutical manufacturing, where powders with passable or better flow properties are preferred for direct compression.

Table 6. Flow properties of MSN-CAF, formulations F1–F4, and formulations N1–N2, determined by angle of repose, Hausner ratio, and Carr’s index (flow characteristics in parentheses). Additionally, B0 represents the blend of excipients (MicroceLac[®] 100, Crospovidone, and Magnesium stearate).

Sample	Angle of Repose	Hausner Ratio	Carr Index
B0	14 (excellent)	1.13 (good)	11 (good)
MSN-NH ₂	61 (very poor)	1.53 (very poor)	35 (very poor)
MSN-CAF	62 (very poor)	1.51 (very poor)	34 (very poor)
F1	12 (excellent)	1.16 (good)	14 (good)
F2	25 (excellent)	1.29 (passable)	22 (passable)
F3	40 (fair)	1.61 (very poor)	33 (very poor)
F4	46 (poor)	1.58 (very, very poor)	38 (very, very poor)
N1	16 (excellent)	1.14 (good)	12 (good)
N2	27 (excellent)	1.28 (passable)	22 (passable)
N3	37 (fair)	1.53 (very poor)	35 (very poor)
N4	55 (poor)	1.65 (very, very poor)	39 (very, ver poor)

Other studies have reported the influence of colloidal silica on powder flow properties; however, most of them utilized low concentrations [16,69,70]. In the present work, we used antioxidant nanomaterial concentrations ranging from 10% to 70%. Additionally, the minimum concentration (10%) of antioxidant nanomaterials ensured a theoretical antioxidant concentration of approximately 1%, which is within the typical range for antioxidant agents in pharmaceutical formulations [71]. The general flow properties of powders containing antioxidant nanomaterials result from particle geometry, friction, and cohesive forces, which are influenced by the distribution of nanoparticles on powder grains. At higher MSN-CAF concentrations, above approximately 30%, nanoparticle agglomeration reduced the free-flowing nature of the powder, impairing its compactability. These findings are critical because they reveal a threshold for suitable flow properties, establishing guidelines for the future design of oral tablets containing nanoantioxidants.

The morphology of the optimal formulation (F1) was examined using scanning electron microscopy. SEM images revealed particles primarily consisting of spherical, porous microagglomerates (Figure 2a) attributable to the characteristic morphology of MicroceLac[®] 100 and crospovidone [72–74]. The spherical particle shape correlates strongly with the excellent flowability observed. Higher-magnification images (Figure 2b) confirmed the presence of MSN-CAF nanoparticles adsorbed on the particle surfaces. Nevertheless, some areas exhibited a higher density of nanoparticles than others (Figure 2c). If the tablet does not disintegrate properly, this agglomeration of nanoparticles could hinder their free movement during the release process, necessitating evaluation based on critical quality attributes.

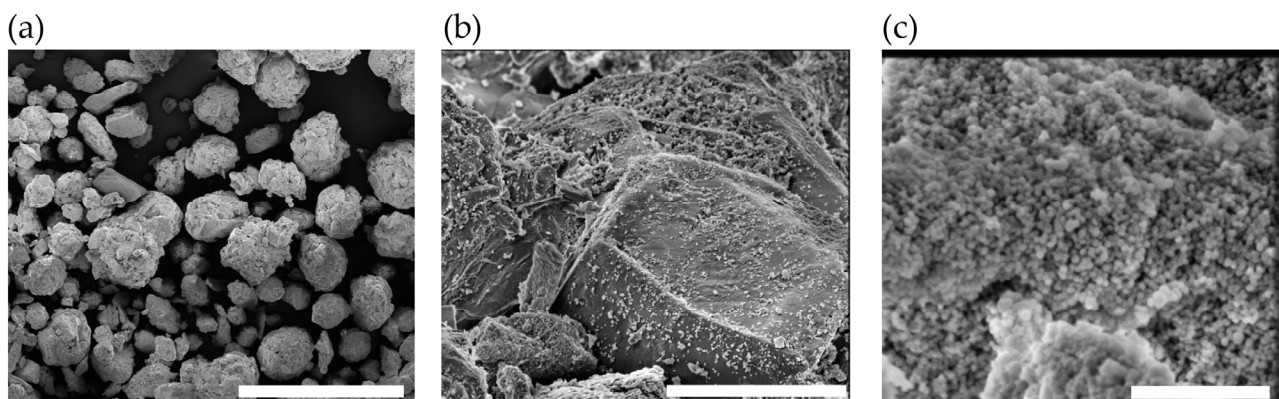


Figure 2. Morphology of the powder of formulation 1. SEM image of (a) formulation F1 (scale bar: 400 μm), (b) F1, magnification of 13,000 \times (scale bar: 10 μm), and (c) F1, magnification of 100,000 \times (scale bar: 1 μm).

3.3. Critical Quality Attributes of Tablets

Based on the results, formulation F1 exhibited the best flow characteristics and was used to manufacture tablets via direct compression. Tablets (124 ± 0.7 mg) were prepared using 5 mm punches (Figure 3a). The diameter and thickness were 4.96 ± 0.02 mm and 5.08 ± 0.04 mm, respectively. Cross-sectional scanning electron microscopy (SEM) images of the tablets (Figure 3b,c) showed that the nanoparticles were completely distributed. These images also confirmed that the morphology of the antioxidant nanomaterial remains intact. Floating tablets consisting of mesoporous silica nanoparticles (MSNs) have been reported [15] exhibiting a similar nanoparticle distribution pattern on the surface of the powder forming the tablet.

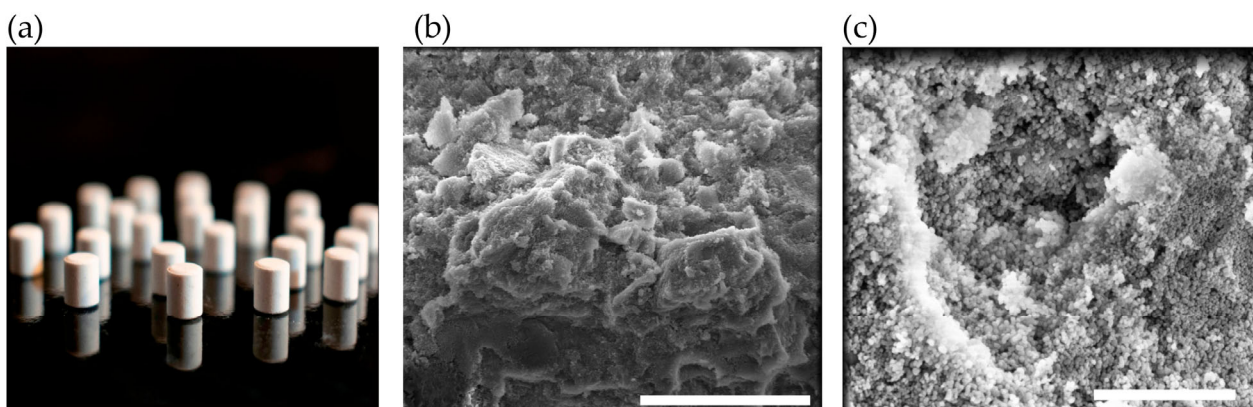


Figure 3. Morphological characteristics of tablets: (a) photograph of the tablet; (b) SEM image of a tablet cross-section (scale bar: 20 μm); (c) SEM image of a tablet cross-section at 50,000 \times magnification (scale bar: 2 μm).

Tablet hardness, defined as the ability to withstand external mechanical forces, is primarily governed by intermolecular forces (e.g., hydrogen bonding, hydrophobic interactions, ionic interactions, and van der Waals forces) and intramolecular forces (e.g., covalent, ionic, and metallic bonds). Appropriate hardness ensures that tablets resist frictional forces during handling while maintaining rapid disintegration upon administration. The average hardness was 66 N, consistent with the typical hardness range reported in the literature [75].

Friability testing revealed a friability of $0.03 \pm 0.01\%$. This result demonstrates that all tested tablets met the United States Pharmacopeia (USP) standards (weight loss $\leq 1\%$), indicating sufficient mechanical strength to withstand stresses such as vibration or abrasion.

The evaluated tablets were formulated for immediate release, lacking coatings or excipients designed to delay disintegration. All tablets exhibited rapid disintegration times of 18 s, meeting USP standards. This performance was attributed to croscopovidone [35]. Alshora et al. (2024) reported disintegration times of 10 s for tablets containing furosemide-loaded nanoparticles formulated with 2% croscopovidone [76]. No statistically significant differences were observed in tablet hardness, friability, or disintegration across all data sets ($p > 0.05$).

Following disintegration, the tablet releases its contents, enabling MSN-CAF to serve functions beyond acting as an excipient to extend product shelf life, such as an antioxidant agent [1,2] or a drug dissolution rate enhancer [14,77]. Whatever the specific requirement, the nanoparticles must be released from the tablet. To measure nanoparticle release, a drug release study was adapted by weighing nanoparticle pellets from aliquots at predetermined time points. The study was conducted in three media mimicking the gastrointestinal environment (pH 1.2, 4.5, and 6.8). According to the release test, nanoparticles were released rapidly, reaching ~87% release at 2 min, ~96% at 5 min, and ~98% at 10 min (Figure 4), indicating nearly complete release within 15 min. Specifically, at 5 min, samples at pH 6.8 and 4.5 showed statistically significant differences in nanoparticle release ($p < 0.05$).

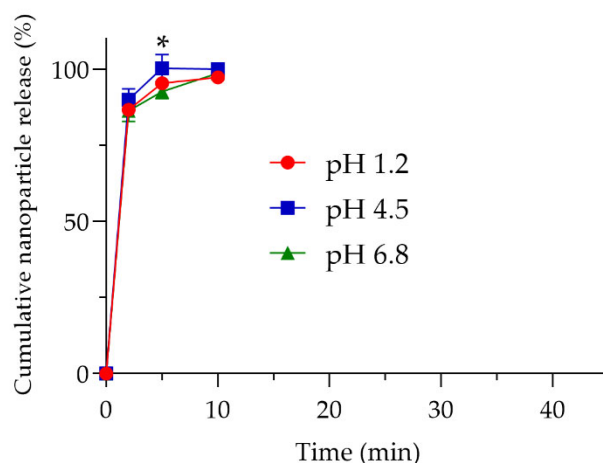


Figure 4. Release profile of the antioxidant nanomaterials. Cumulative nanoparticle release (%) at pH 1.2 (red line), pH 4.5 (blue line), and pH 6.8 (green line). Experiments were performed in triplicate ($n = 3$). * $p < 0.05$ between pH 6.8 and pH 4.5 at 5 min.

Nonetheless, the overall results indicated that the nanoparticles were released almost immediately upon contact with simulated gastrointestinal fluids. This rapid release ensures that any subsequent release of a bioactive compound would depend solely on the nanoparticle design and release mechanism rather than being limited by interactions between the nanoparticles and the tablet matrix. The morphology and textural parameters of nanoparticles after the release test were evaluated. The results showed no significant changes (Figures S1 and S2 and Table S1). Taken together, these results demonstrate the successful incorporation of MSN-CAF into oral tablets via direct compression, with suitable critical quality attributes for use as an excipient, drug carrier, antioxidant, or shelf-life extender.

3.4. In Vitro Cytotoxicity Studies

The excipients in the formulation are well-established, with demonstrated biosafety, and are widely used in pharmaceutical products. Additionally, caffeic acid exhibits hepatoprotective effects [78]. However, the antioxidant nanomaterial described herein requires thorough biocompatibility evaluation. Therefore, we conducted an MTT assay using HepG2 cells, selected for their relevance to the potential oral administration route, to assess the

nanomaterial's biocompatibility. Exposure of HepG2 cells to either MSN-NH₂ or MSN-CAF for up to 48 h did not compromise cellular metabolic activity (Figure 5).

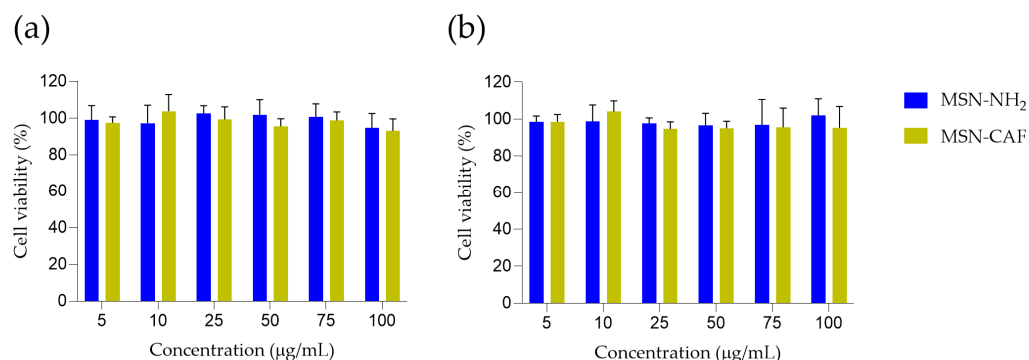


Figure 5. MTT-based analysis of HepG2 cell viability in response to MSN-NH₂ and MSN-CAF treatments. HepG2 Cells were incubated for (a) 24 and (b) 48 h with increasing concentrations (5–100 µg/mL) of each formulation. Cell viability was assessed using the MTT assay and expressed as a percentage relative to the untreated control group. Values are presented as mean ± standard deviation from three independent experiments, each performed in triplicate (n = 3). No significant differences were observed between treated and control groups at any concentration or time point (two-way ANOVA, $p > 0.05$).

Mean viabilities at 24 h ranged from 95% to 105% for MSN-NH₂ and 93% to 104% for MSN-CAF across the concentration range tested. A similar pattern was observed at 48 h, with average values between 97% and 102% for MSN-NH₂ and 95% to 104% for MSN-CAF. No dose-dependent decline was detected, and statistical analysis revealed no significant differences between treatments groups at any time point ($p > 0.05$). The results demonstrate that HepG2 hepatocytes maintain normal metabolic activity in the presence of both nanoparticle systems at the evaluated doses, suggesting their safety and biocompatibility. These findings are consistent with previous reports on silica-based nanomaterials [79–81].

4. Conclusions

This study demonstrates the successful incorporation of an antioxidant nanomaterial based on mesoporous silica functionalized with caffeic acid (MSN-CAF) into oral tablets via direct compression, highlighting their potential as a multifunctional platform in pharmaceutical, nutraceutical, and food applications. The reduced antioxidant capacity of MSN-CAF compared with free caffeic acid, observed in DPPH•, ABTS•⁺, ORAC, and FRAP assays, suggested limited surface availability due to pore entrapment, yet sufficient activity remained for practical applications. Higher concentrations of the antioxidant nanomaterial in tablet formulations, particularly above approximately 30%, significantly influenced powder flow properties. Specifically, formulation F1 (10% MSN-CAF) exhibited excellent flowability, making it suitable for industrial tablet manufacturing. Furthermore, tablets produced with F1 demonstrated robust critical quality attributes, including rapid disintegration, low friability, and high nanoparticle release. Additionally, an in vitro cytotoxicity assay suggested the biocompatibility of the antioxidant nanomaterial. These results confirm that MSN-CAF can simultaneously function as a pharmaceutical excipient, antioxidant agent, and delivery system. This opens opportunities for its application in active packaging, nutraceuticals, pharmaceuticals, and functional foods, where protection of oxidation-sensitive compounds and controlled release provide added value. Future research could explore other polyphenols, nonporous matrices, or stimuli-responsive systems to optimize bioactive release and expand industrial applications.

Supplementary Materials: The following supporting information can be downloaded at: <https://www.mdpi.com/article/10.3390/antiox14070829/s1>. Table S1. Textural properties of nanoparticles after release studies at different pH values. Figure S1. SEM images of MSN-CAF after the release study at (a) pH 1.2, (b) pH 4.5, (c) pH 6.8, and (d) pH 6.8 after 5 h. The scale bars in (a–c) represent 5 μm , and in (d) represent 1 μm . Figure S2. N_2 adsorption/desorption isotherms of MSN-CAF after the release study at (a) pH 1.2, (b) pH 4.5, (c) pH 6.8, and (d) pH 6.8 after 5 h.

Author Contributions: Conceptualization, A.C.O. and F.A.; methodology, A.C.O., M.J.S., C.F.L. and F.A.; software, S.P., D.R., J.C.-R. and F.A.; validation, A.C.O., J.M., M.J.S., C.F.L. and F.A.; formal analysis, J.C.-R., L.R.-Q., D.R. and F.A.; investigation, J.C.-R., L.R.-Q., D.R., S.P., A.C.O., M.J.S. and F.A.; resources, A.C.O., M.J.S., J.M., C.F.L. and F.A.; data curation, F.A.; writing—original draft preparation, A.C.O. and F.A.; writing—review and editing, A.C.O., J.C.-R., L.R.-Q., C.F.L., S.P., D.R., M.J.S., J.M. and F.A.; visualization, A.C.O. and F.A.; supervision, A.C.O., M.J.S. and F.A.; project administration, F.A.; funding acquisition, A.C.O., M.J.S., J.M., C.F.L. and F.A. All authors have read and agreed to the published version of the manuscript.

Funding: This research was supported by ANID/FONDECYT iniciación 11200194 (F.A.), ANID/FONDECYT iniciación 11240466 (A.C.O.), ANID/FONDECYT regular 1221145 (J.M.), and ANID/FONDECYT regular 1220055 (M.J.S.).

Institutional Review Board Statement: Not applicable.

Informed Consent Statement: Not applicable.

Data Availability Statement: The manuscript and Supplementary Materials contain the reported data. Additional relevant data can be obtained upon request from the corresponding author.

Acknowledgments: The authors acknowledge the support of the FONDEQUIP EQM170111.

Conflicts of Interest: The authors declare no conflicts of interest.

References

1. Shah, S.T.; Chowdhury, Z.Z.; Simarani, K.; Basirun, W.J.; Badruddin, I.A.; Hussien, M.; Alrobei, H.; Kamangar, S. Nanoantioxidants: The Fourth Generation of Antioxidants—Recent Research Roadmap and Future Perspectives. *Coatings* **2022**, *12*, 1568. [[CrossRef](#)]
2. Khalil, I.; Yehye, W.A.; Etxeberria, A.E.; Alhadi, A.A.; Dezfooli, S.M.; Julkapli, N.B.M.; Basirun, W.J.; Seyfoddin, A. Nanoantioxidants: Recent Trends in Antioxidant Delivery Applications. *Antioxidants* **2020**, *9*, 24. [[CrossRef](#)] [[PubMed](#)]
3. Munin, A.; Edwards-Lévy, F. Encapsulation of Natural Polyphenolic Compounds; a Review. *Pharmaceutics* **2011**, *3*, 793–829. [[CrossRef](#)] [[PubMed](#)]
4. Omran, B.; Baek, K.-H. Nanoantioxidants: Pioneer Types, Advantages, Limitations, and Future Insights. *Molecules* **2021**, *26*, 7031. [[CrossRef](#)]
5. Cheng, Y.; Cai, S.; Wu, H.; Pan, J.; Su, M.; Wei, X.; Ye, J.; Ke, L.; Liu, G.; Chu, C. Revolutionizing Eye Care: The Game-Changing Applications of Nano-Antioxidants in Ophthalmology. *Nanoscale* **2024**, *16*, 7307–7322. [[CrossRef](#)]
6. Eftekhari, A.; Dizaj, S.M.; Chodari, L.; Sunar, S.; Hasanzadeh, A.; Ahmadian, E.; Hasanzadeh, M. The Promising Future of Nano-Antioxidant Therapy against Environmental Pollutants Induced-Toxicities. *Biomed. Pharmacother.* **2018**, *103*, 1018–1027. [[CrossRef](#)]
7. Birinci, Y.; Niazi, J.H.; Aktay-Çetin, O.; Basaga, H. Quercetin in the Form of a Nano-Antioxidant (QTiO₂) Provides Stabilization of Quercetin and Maximizes Its Antioxidant Capacity in the Mouse Fibroblast Model. *Enzyme Microb. Technol.* **2020**, *138*, 109559. [[CrossRef](#)]
8. Shah, S.T.; Chowdhury, Z.Z.; Johan, M.R.B.; Badruddin, I.A.; Khaleed, H.M.T.; Kamangar, S.; Alrobei, H. Surface Functionalization of Magnetite Nanoparticles with Multipotent Antioxidant as Potential Magnetic Nanoantioxidants and Antimicrobial Agents. *Molecules* **2022**, *27*, 789. [[CrossRef](#)]
9. Martakov, I.S.; Shevchenko, O.G.; Torlopov, M.A.; Sitnikov, P.A. Colloidally Stable Conjugates of Phenolic Acids with γ -AlOOH Nanoparticles as Efficient and Biocompatible Nanoantioxidants. *J. Mol. Struct.* **2022**, *1248*, 131471. [[CrossRef](#)]
10. Meshkini, A.; Khoshshokhan, F. Transformative Nanoantioxidant Chitosan Films: High-Performance Active Packaging with Minimal Cytotoxicity. *Int. J. Biol. Macromol.* **2025**, *304*, 140983. [[CrossRef](#)]
11. Baumgartner, A.; Planinšek, O. Application of Commercially Available Mesoporous Silica for Drug Dissolution Enhancement in Oral Drug Delivery. *Eur. J. Pharm. Sci.* **2021**, *167*, 106015. [[CrossRef](#)]

12. Fatima, R.; Katiyar, P.; Kushwaha, K. Recent Advances in Mesoporous Silica Nanoparticle: Synthesis, Drug Loading, Release Mechanisms, and Diverse Applications. *Front. Nanotechnol.* **2025**, *7*, 1564188. [[CrossRef](#)]
13. Ibrahim, A.H.; Smått, J.-H.; Govardhanam, N.P.; Ibrahim, H.M.; Ismael, H.R.; Afouna, M.I.; Samy, A.M.; Rosenholm, J.M. Formulation and Optimization of Drug-Loaded Mesoporous Silica Nanoparticle-Based Tablets to Improve the Dissolution Rate of the Poorly Water-Soluble Drug Silymarin. *Eur. J. Pharm. Sci.* **2020**, *142*, 105103. [[CrossRef](#)] [[PubMed](#)]
14. Kim, D.; Koo, J.; Yang, E.-J.; Shim, K.; Tin, Y.Y.; Lin, Z.; Oh, K.T.; Na, D.H. Entrapment of Celecoxib into Mesoporous Silica Particles for Tablets with Improved Dissolution through Amorphization. *J. Drug Deliv. Sci. Technol.* **2023**, *84*, 104485. [[CrossRef](#)]
15. Abbaraju, P.L.; Meka, A.K.; Jambhrunkar, S.; Zhang, J.; Xu, C.; Popat, A.; Yu, C. Floating Tablets from Mesoporous Silica Nanoparticles. *J. Mater. Chem. B* **2014**, *2*, 8298–8302. [[CrossRef](#)]
16. Lumay, G.; Pillitteri, S.; Marck, M.; Monsuur, F.; Pauly, T.; Ribeyre, Q.; Francqui, F.; Vandewalle, N. Influence of Mesoporous Silica on Powder Flow and Electrostatic Properties on Short and Long Term. *J. Drug Deliv. Sci. Technol.* **2019**, *53*, 101192. [[CrossRef](#)]
17. Lumay, G.; Boschini, F.; Traina, K.; Bontempi, S.; Remy, J.-C.; Cloots, R.; Vandewalle, N. Measuring the Flowing Properties of Powders and Grains. *Powder Technol.* **2012**, *224*, 19–27. [[CrossRef](#)]
18. Ehtiati, S.; Alizadeh, M.; Farhadi, F.; Khalatbari, K.; Ajiboye, B.O.; Baradaran Rahimi, V.; Askari, V.R. Promising Influences of Caffeic Acid and Caffeic Acid Phenethyl Ester against Natural and Chemical Toxins: A Comprehensive and Mechanistic Review. *J. Funct. Foods* **2023**, *107*, 105637. [[CrossRef](#)]
19. Purushothaman, A.; Babu, S.S.; Naroth, S.; Janardanan, D. Antioxidant Activity of Caffeic Acid: Thermodynamic and Kinetic Aspects on the Oxidative Degradation Pathway. *Free Radic. Res.* **2022**, *56*, 617–630. [[CrossRef](#)]
20. Gălbău, C.Ș.; Badea, M.; Gaman, L.E. Do Young Consumers Care about Antioxidant Benefits and Resveratrol and Caffeic Acid Consumption? *Nutrients* **2024**, *16*, 1439. [[CrossRef](#)]
21. Symes, A.; Shavandi, A.; Zhang, H.; Mohamed Ahmed, I.A.; Al-Juhaimi, F.Y.; Bekhit, A.E.-D.A. Antioxidant Activities and Caffeic Acid Content in New Zealand Asparagus (*Asparagus officinalis*) Roots Extracts. *Antioxidants* **2018**, *7*, 52. [[CrossRef](#)] [[PubMed](#)]
22. Taysi, S.; Algburi, F.S.; Taysi, M.E.; Caglayan, C. Caffeic Acid Phenethyl Ester: A Review on Its Pharmacological Importance, and Its Association with Free Radicals, COVID-19, and Radiotherapy. *Phytother. Res.* **2023**, *37*, 1115–1135. [[CrossRef](#)] [[PubMed](#)]
23. Cortez, N.; Villegas, C.; Burgos, V.; Cabrera-Pardo, J.R.; Ortiz, L.; González-Chavarría, I.; Nchiozem-Ngnitedem, V.-A.; Paz, C. Adjuvant Properties of Caffeic Acid in Cancer Treatment. *Int. J. Mol. Sci.* **2024**, *25*, 7631. [[CrossRef](#)]
24. Alpsoy, L.; Baykal, A.; Kurtan, U.; Akal, Z.Ü. Superparamagnetic Iron Oxide Nanoparticles (SPION) Functionalized by Caffeic Acid (CFA). *J. Supercond. Nov. Magn.* **2017**, *30*, 2699–2706. [[CrossRef](#)]
25. İlyasoğlu, H.; Nadzieja, M.; Guo, Z. Caffeic Acid Grafted Chitosan as a Novel Dual-Functional Stabilizer for Food-Grade Emulsions and Additive Antioxidant Property. *Food Hydrocoll.* **2019**, *95*, 168–176. [[CrossRef](#)]
26. Klein, S.; Smuda, M.; Harreiß, C.; Menter, C.; Distel, L.V.R.; Kryschi, C. Bifunctional Au-Fe₃O₄ Nanoheterodimers Acting as X-Ray Protector in Healthy Cells and as X-Ray Enhancer in Tumor Cells. *ACS Appl. Mater. Interfaces* **2019**, *11*, 39613–39623. [[CrossRef](#)]
27. Mazzotta, E.; Orlando, C.; Muzzalupo, R. New Nanomaterials with Intrinsic Antioxidant Activity by Surface Functionalization of Niosomes with Natural Phenolic Acids. *Pharmaceutics* **2021**, *13*, 766. [[CrossRef](#)]
28. Chen, J.; Yang, J.; Ma, L.; Li, J.; Shahzad, N.; Kim, C.K. Structure-Antioxidant Activity Relationship of Methoxy, Phenolic Hydroxyl, and Carboxylic Acid Groups of Phenolic Acids. *Sci. Rep.* **2020**, *10*, 2611. [[CrossRef](#)]
29. Teixeira, J.; Gaspar, A.; Garrido, E.M.; Garrido, J.; Borges, F. Hydroxycinnamic Acid Antioxidants: An Electrochemical Overview. *BioMed Res. Int.* **2013**, *2013*, 251754. [[CrossRef](#)]
30. Jia, C.-H.; Wang, X.-Y.; Qi, J.-F.; Hong, S.-T.; Lee, K.-T. Antioxidant Properties of Caffeic Acid Phenethyl Ester and 4-Vinylcatechol in Stripped Soybean Oil. *J. Food Sci.* **2016**, *81*, C35–C41. [[CrossRef](#)]
31. Hao, N.; Jayawardana, K.W.; Chen, X.; Yan, M. One-Step Synthesis of Amine-Functionalized Hollow Mesoporous Silica Nanoparticles as Efficient Antibacterial and Anticancer Materials. *ACS Appl. Mater. Interfaces* **2015**, *7*, 1040–1045. [[CrossRef](#)] [[PubMed](#)]
32. Arriagada, F.; Günther, G.; Nos, J.; Nonell, S.; Olea-Azar, C.; Morales, J. Antioxidant Nanomaterial Based on Core-Shell Silica Nanospheres with Surface-Bound Caffeic Acid: A Promising Vehicle for Oxidation-Sensitive Drugs. *Nanomaterials* **2019**, *9*, 214. [[CrossRef](#)] [[PubMed](#)]
33. Saha, S.; and Shahiwala, A.F. Multifunctional Coprocessed Excipients for Improved Tableting Performance. *Expert Opin. Drug Deliv.* **2009**, *6*, 197–208. [[CrossRef](#)]
34. Michoel, A.; Rombaut, P.; Verhoye, A. Comparative Evaluation of Co-Processed Lactose and Microcrystalline Cellulose with Their Physical Mixtures in the Formulation of Folic Acid Tablets. *Pharm. Dev. Technol.* **2002**, *7*, 79–87. [[CrossRef](#)] [[PubMed](#)]
35. Desai, P.M.; Liew, C.V.; Heng, P.W.S. Review of Disintegrants and the Disintegration Phenomena. *J. Pharm. Sci.* **2016**, *105*, 2545–2555. [[CrossRef](#)]

36. Martínez-Acevedo, L.; de la Luz Zambrano-Zaragoza, M.; Vidal-Romero, G.; Mendoza-Elvira, S.; Quintanar-Guerrero, D. Evaluation of the Lubricating Effect of Magnesium Stearate and Glyceryl Behenate Solid Lipid Nanoparticles in a Direct Compression Process. *Int. J. Pharm.* **2018**, *545*, 170–175. [[CrossRef](#)]
37. Martínez-Acevedo, L.; Job Galindo-Pérez, M.; Vidal-Romero, G.; del Real, A.; de la Luz Zambrano-Zaragoza, M.; Quintanar-Guerrero, D. Effect of Magnesium Stearate Solid Lipid Nanoparticles as a Lubricant on the Properties of Tablets by Direct Compression. *Eur. J. Pharm. Biopharm.* **2023**, *193*, 262–273. [[CrossRef](#)]
38. Haruna, F.; Apeji, Y.E.; Oparaache, C.; Oyi, A.R.; Gamlen, M. Compaction and Tableting Properties of Composite Particles of Microcrystalline Cellulose and Crospovidone Engineered for Direct Compression. *Future J. Pharm. Sci.* **2020**, *6*, 35. [[CrossRef](#)]
39. Tafere, C.; Yilma, Z.; Abrha, S.; Yehualaw, A. Formulation, in Vitro Characterization and Optimization of Taste-Masked Orally Disintegrating Co-Trimoxazole Tablet by Direct Compression. *PLoS ONE* **2021**, *16*, e0246648. [[CrossRef](#)]
40. Teżyk, M.; Jakubowska, E.; Milczewska, K.; Milanowski, B.; Voelkel, A.; Lulek, J. The Influence of Direct Compression Powder Blend Transfer Method from the Container to the Tablet Press on Product Critical Quality Attributes: A Case Study. *Drug Dev. Ind. Pharm.* **2017**, *43*, 911–916. [[CrossRef](#)]
41. Torres-Benítez, A.; Ortega-Valencia, J.E.; Flores-González, M.; Sánchez, M.; Simirgiotis, M.J.; Gómez-Serranillos, M.P. Phytochemical Characterization and In Vitro and In Silico Biological Studies from Ferns of Genus *Blechnum* (Blechnaceae, Polypodiales). *Antioxidants* **2023**, *12*, 540. [[CrossRef](#)]
42. Hopfstock, P.; Romero-Parra, J.; Winterhalter, P.; Gök, R.; Simirgiotis, M. In Vitro Inhibition of Enzymes and Antioxidant and Chemical Fingerprinting Characteristics of *Azara serrata* Ruiz & Pav. Fruits, an Endemic Plant of the Valdivian Forest of Chile. *Plants* **2024**, *13*, 2756. [[CrossRef](#)]
43. Viteri, R.; Espinoza, F.; Cornejo, X.; Simirgiotis, M.J.; Manzano, P. Phytochemical Profiling, Antioxidant, Enzymatic Inhibitory, and Antibacterial Activities of *Wigandia Ecuadorensis*. *Front. Plant Sci.* **2024**, *15*, 1481447. [[CrossRef](#)] [[PubMed](#)]
44. USP. <1174> Powder Flow. In *USP–NF*; USP: Rockville, MD, USA, 2024.
45. Boyd, B.J.; Bergström, C.A.S.; Vinarov, Z.; Kuentz, M.; Brouwers, J.; Augustijns, P.; Brandl, M.; Bernkop-Schnürch, A.; Shrestha, N.; Prêat, V.; et al. Successful Oral Delivery of Poorly Water-Soluble Drugs Both Depends on the Intraluminal Behavior of Drugs and of Appropriate Advanced Drug Delivery Systems. *Eur. J. Pharm. Sci.* **2019**, *137*, 104967. [[CrossRef](#)] [[PubMed](#)]
46. USP. Propranolol Hydrochloride Extended-Release Capsules. In *USP–NF*; USP: Rockville, MD, USA, 2020.
47. USP. Methazolamide Tablets. In *USP–NF*; USP: Rockville, MD, USA, 2020.
48. Shafqat, S.S.; Khan, A.A.; Zafar, M.N.; Alhaji, M.H.; Sanullah, K.; Shafqat, S.R.; Murtaza, S.; Pang, S.C. Development of Amino-Functionalized Silica Nanoparticles for Efficient and Rapid Removal of COD from Pre-Treated Palm Oil Effluent. *J. Mater. Res. Technol.* **2019**, *8*, 385–395. [[CrossRef](#)]
49. Ebabe Elle, R.; Rahmani, S.; Lauret, C.; Morena, M.; Bidel, L.P.R.; Boulahtouf, A.; Balaguer, P.; Cristol, J.-P.; Durand, J.-O.; Charnay, C.; et al. Functionalized Mesoporous Silica Nanoparticle with Antioxidants as a New Carrier That Generates Lower Oxidative Stress Impact on Cells. *Mol. Pharm.* **2016**, *13*, 2647–2660. [[CrossRef](#)]
50. Deligiannakis, Y.; Sotiriou, G.A.; Pratsinis, S.E. Antioxidant and Antiradical SiO₂ Nanoparticles Covalently Functionalized with Gallic Acid. *ACS Appl. Mater. Interfaces* **2012**, *4*, 6609–6617. [[CrossRef](#)]
51. Avendaño-Godoy, J.; Cattoën, X.; Kogan, M.J.; Morales Valenzuela, J. Epigallocatechin-3-Gallate Adsorbed on Core-Shell Gold Nanorod@mesoporous Silica Nanoparticles, an Antioxidant Nanomaterial with Photothermal Properties. *Int. J. Pharm.* **2024**, *662*, 124507. [[CrossRef](#)]
52. Trendafilova, I.; Lazarova, H.; Chimshirova, R.; Trusheva, B.; Koseva, N.; Popova, M. Novel Kaempferol Delivery Systems Based on Mg-Containing MCM-41 Mesoporous Silicas. *J. Solid State Chem.* **2021**, *301*, 122323. [[CrossRef](#)]
53. Spagnol, C.M.; Assis, R.P.; Brunetti, I.L.; Isaac, V.L.B.; Salgado, H.R.N.; Corrêa, M.A. In Vitro Methods to Determine the Antioxidant Activity of Caffeic Acid. *Spectrochim. Acta A Mol. Biomol. Spectrosc.* **2019**, *219*, 358–366. [[CrossRef](#)]
54. Mazzone, G.; Russo, N.; Toscano, M. Antioxidant Properties Comparative Study of Natural Hydroxycinnamic Acids and Structurally Modified Derivatives: Computational Insights. *Comput. Theor. Chem.* **2016**, *1077*, 39–47. [[CrossRef](#)]
55. Xie, J.; Schaich, K.M. Re-Evaluation of the 2,2-Diphenyl-1-Picrylhydrazyl Free Radical (DPPH) Assay for Antioxidant Activity. *J. Agric. Food Chem.* **2014**, *62*, 4251–4260. [[CrossRef](#)] [[PubMed](#)]
56. Leopoldini, M.; Russo, N.; Toscano, M. The Molecular Basis of Working Mechanism of Natural Polyphenolic Antioxidants. *Food Chem.* **2011**, *125*, 288–306. [[CrossRef](#)]
57. Schaich, K.M.; Tian, X.; Xie, J. Hurdles and Pitfalls in Measuring Antioxidant Efficacy: A Critical Evaluation of ABTS, DPPH, and ORAC Assays. *J. Funct. Foods* **2015**, *14*, 111–125. [[CrossRef](#)]
58. Trendafilova, I.; Mihály, J.; Momekova, D.; Chimshirova, R.; Lazarova, H.; Momekov, G.; Popova, M. Antioxidant Activity and Modified Release Profiles of Morin and Hesperetin Flavonoids Loaded in Mg-or Ag-Modified SBA-16 Carriers. *Today Commun.* **2020**, *24*, 101198. [[CrossRef](#)]
59. Catauro, M.; Barrino, F.; Dal Poggetto, G.; Crescente, G.; Piccolella, S.; Pacifico, S. New SiO₂/Caffeic Acid Hybrid Materials: Synthesis, Spectroscopic Characterization, and Bioactivity. *Materials* **2020**, *13*, 394. [[CrossRef](#)] [[PubMed](#)]

60. Catauro, M.; Poggetto, G.D.; Crescente, G.; Piccolella, S.; Pacifico, S. Cytocompatibility of Caffeic Acid-Silica Hybrid Materials on NIH-3T3 Fibroblast Cells. *Macromol. Symp.* **2021**, *395*, 2000205. [[CrossRef](#)]
61. Berlier, G.; Gastaldi, L.; Ugazio, E.; Miletto, I.; Iliade, P.; Sapino, S. Stabilization of Quercetin Flavonoid in MCM-41 Mesoporous Silica: Positive Effect of Surface Functionalization. *J. Colloid Interface Sci.* **2013**, *393*, 109–118. [[CrossRef](#)]
62. Gonnissen, Y.; Remon, J.P.; Vervaet, C. Development of Directly Compressible Powders via Co-Spray Drying. *Eur. J. Pharm. Biopharm.* **2007**, *67*, 220–226. [[CrossRef](#)]
63. Morin, G.; Briens, L. The Effect of Lubricants on Powder Flowability for Pharmaceutical Application. *AAPS PharmSciTech* **2013**, *14*, 1158–1168. [[CrossRef](#)]
64. Yavari, A.; Sadjady, S.K.; Moniri, E.; Nokhodchi, A.; Haghighat Talab, F. Investigating the Influence of Crospovidone's Manufacturer Variability on Dissolution Profiles of Hydrochlorothiazide Tablets. *AAPS PharmSciTech* **2025**, *26*, 52. [[CrossRef](#)]
65. Saker, A.; Cares-Pacheco, M.-G.; Marchal, P.; Falk, V. Powders Flowability Assessment in Granular Compaction: What about the Consistency of Hausner Ratio? *Powder Technol.* **2019**, *354*, 52–63. [[CrossRef](#)]
66. Voycheva, C.; Tzankov, B.; Tzankova, D.G.; Avramova, K.I.; Yoncheva, K.P. Formulation of Tablets Containing Glimepiride-Loaded Mesoporous Silica Particles. *Indian J. Pharm. Sci.* **2019**, *81*, 483–488. [[CrossRef](#)]
67. Wang, Z.; Ye, B.-N.; Zhang, Y.-T.; Xie, J.-X.; Li, W.-S.; Zhang, H.-T.; Liu, Y.; Feng, N.-P. Exploring the Potential of Mesoporous Silica as a Carrier for Puerarin: Characterization, Physical Stability, and In Vivo Pharmacokinetics. *AAPS PharmSciTech* **2019**, *20*, 289. [[CrossRef](#)]
68. Zhang, Y.; Li, Y.; Wu, F.; Hong, Y.; Shen, L.; Lin, X.; Feng, Y. Texture and Surface Feature-Mediated Striking Improvements on Multiple Direct Compaction Properties of *Zingiberis Rhizoma* Extracted Powder by Coprocessing with Nano-Silica. *Int. J. Pharm.* **2021**, *603*, 120703. [[CrossRef](#)]
69. Majerová, D.; Kulaviak, L.; Růžička, M.; Štěpánek, F.; Zámotný, P. Effect of Colloidal Silica on Rheological Properties of Common Pharmaceutical Excipients. *Eur. J. Pharm. Biopharm.* **2016**, *106*, 2–8. [[CrossRef](#)] [[PubMed](#)]
70. Blanco, D.; Antikainen, O.; Rääkkönen, H.; Yliruusi, J.; Juppo, A.M. Effect of Colloidal Silicon Dioxide and Moisture on Powder Flow Properties: Predicting in-Process Performance Using Image-Based Analysis. *Int. J. Pharm.* **2021**, *597*, 120344. [[CrossRef](#)] [[PubMed](#)]
71. Celestino, M.T.; de Oliveira Magalhães, U.; Fraga, A.G.M.; do Carmo, F.A.; Lione, V.; Castro, H.C.; de Sousa, V.P.; Rodrigues, C.R.; Cabral, L.M. Rational Use of Antioxidants in Solid Oral Pharmaceutical Preparations. *Braz. J. Pharm. Sci.* **2012**, *48*, 405–415. [[CrossRef](#)]
72. Haware, R.V.; Kancharla, J.P.; Udupa, A.K.; Staton, S.; Gupta, M.R.; Al-Achi, A.; Stagner, W.C. Physico-Mechanical Properties of Coprocessed Excipient MicroceLac® 100 by DM3 Approach. *Pharm. Res.* **2015**, *32*, 3618–3635. [[CrossRef](#)]
73. Dominik, M.; Vraníková, B.; Svačinová, P.; Elbl, J.; Pavloková, S.; Prudilová, B.B.; Šklubalová, Z.; Franc, A. Comparison of Flow and Compression Properties of Four Lactose-Based Co-Processed Excipients: Cellactose® 80, CombiLac®, MicroceLac® 100, and StarLac®. *Pharmaceutics* **2021**, *13*, 1486. [[CrossRef](#)]
74. Steffens, K.E.; Wagner, K.G. Immediate-Release Formulations Produced via Twin-Screw Melt Granulation: Systematic Evaluation of the Addition of Disintegrants. *AAPS PharmSciTech* **2021**, *22*, 183. [[CrossRef](#)]
75. Porter, S.; Sackett, G.; Liu, L. Chapter 34—Development, Optimization, and Scale-Up of Process Parameters: Pan Coating. In *Developing Solid Oral Dosage Forms*, 2nd ed.; Qiu, Y., Chen, Y., Zhang, G.G.Z., Yu, L., Mantri, R.V., Eds.; Academic Press: Boston, MA, USA, 2017; pp. 953–996, ISBN 978-0-12-802447-8.
76. Alshora, D.; Alyousef, W.; Ibrahim, M. Effects of Functional Biomaterials on the Attributes of Orally Disintegrating Tablets Loaded with Furosemide Nanoparticles: In Vitro and In Vivo Evaluations. *J. Funct. Biomater.* **2024**, *15*, 161. [[CrossRef](#)] [[PubMed](#)]
77. Arriagada, F.; Günther, G.; Morales, J. Nanoantioxidant-Based Silica Particles as Flavonoid Carrier for Drug Delivery Applications. *Pharmaceutics* **2020**, *12*, 302. [[CrossRef](#)] [[PubMed](#)]
78. Tsai, T.-H.; Yu, C.-H.; Chang, Y.-P.; Lin, Y.-T.; Huang, C.-J.; Kuo, Y.-H.; Tsai, P.-J. Protective Effect of Caffeic Acid Derivatives on Tert-Butyl Hydroperoxide-Induced Oxidative Hepato-Toxicity and Mitochondrial Dysfunction in HepG2 Cells. *Molecules* **2017**, *22*, 702. [[CrossRef](#)]
79. AbouAitah, K.; Swiderska-Sroda, A.; Farghali, A.A.; Wojnarowicz, J.; Stefanek, A.; Gierlotka, S.; Opalinska, A.; Allayeh, A.K.; Ciach, T.; Lojkowski, W. Folic Acid-Conjugated Mesoporous Silica Particles as Nanocarriers of Natural Prodrugs for Cancer Targeting and Antioxidant Action. *Oncotarget* **2018**, *9*, 26466–26490. [[CrossRef](#)] [[PubMed](#)]
80. Bhavsar, D.; Patel, V.; Sawant, K. Systematic Investigation of *in Vitro* and *in Vivo* Safety, Toxicity and Degradation of Mesoporous Silica Nanoparticles Synthesized Using Commercial Sodium Silicate. *Microporous Mesoporous Mater.* **2019**, *284*, 343–352. [[CrossRef](#)]
81. Elbially, N.S.; Aboushoushah, S.F.; Sofi, B.F.; Noorwali, A. Multifunctional Curcumin-Loaded Mesoporous Silica Nanoparticles for Cancer Chemoprevention and Therapy. *Microporous Mesoporous Mater.* **2020**, *291*, 109540. [[CrossRef](#)]

Disclaimer/Publisher's Note: The statements, opinions and data contained in all publications are solely those of the individual author(s) and contributor(s) and not of MDPI and/or the editor(s). MDPI and/or the editor(s) disclaim responsibility for any injury to people or property resulting from any ideas, methods, instructions or products referred to in the content.